Pressure loss in channel flow resulting from a sudden change in boundary condition from no-slip to partial-slip

Chiu-On Ng[a] and Rui Sun
Department of Mechanical Engineering, The University of Hong Kong, Pokfulam Road, Hong Kong

(Received 3 June 2017; accepted 22 September 2017; published online 9 October 2017)

A semi-analytical model is presented for pressure-driven flow through a channel, where local pressure loss is incurred at a sudden change in the boundary condition: from no-slip to partial-slip. Assuming low-Reynolds-number incompressible flow and periodic stick–slip wall patterning, the problems for parallel-plate and circular channels are solved using the methods of eigenfunction expansion and point match. The present study aims to examine in detail how the flow will evolve, on passing through the cross section at which the change in the slip condition occurs, from a no-slip parabolic profile to a less sheared profile with a boundary slip. The present problem is germane to, among other applications, flow through a channel bounded by superhydrophobic surfaces, which intrinsically comprise an array of no-slip and partial-slip segments. Results are presented to show that the sudden change in the boundary condition will result in additional resistance to the flow. Near the point on the wall where a slip change occurs is a region of steep pressure gradient and intensive vorticity. The acceleration of near-wall fluid particles in combination with the no-slip boundary condition leads to a very steep velocity gradient at the wall, thereby a sharp increase in the wall shear stress, shortly before the fluid enters the channel with a slippery wall. Results are also presented to show the development of flow in the entrance region in the slippery channel. The additional pressure loss can be represented by a dimensionless loss parameter, which is a pure function of the slip length for channels much longer than the entrance length. *Published by AIP Publishing.* https://doi.org/10.1063/1.4986268

I. INTRODUCTION

Pressure or head loss in pipe flow can be classified into friction and minor losses. Friction loss arises from wall skin friction, stemming from fluid's viscosity and the condition of no-slip on the wall. It is linearly proportional to the length of the pipe, and hence in long pipe systems, it is usually the major cause of pressure loss. Minor losses are local pressure drops incurred at changes in the cross sections, bends, valves, fittings, and so on. In pipe systems with short runs of a straight pipe, the total minor loss may outweigh the friction loss. Therefore, the effect of a minor loss is not necessarily minor. Minor loss is also called additional loss.[1]

In this paper, we look into a kind of additional loss that has not received much attention thus far. This kind of loss is not due to a change in the channel geometry but due to a change in the slip condition on the boundary. Our problem is to consider a low-Reynolds-number flow through a long and straight channel with a uniform cross section, where at a certain axial position the channel wall undergoes a step change in the slip condition, from being no-slip to partial-slip. We shall show that there is a pressure drop associated with such a step change in the slip condition. The problem is of relevance to flow in channels of typical dimensions on the order of microns or smaller.

Many controlled experiments have demonstrated an apparent violation of the no-slip boundary condition for flow of a liquid over a solid surface in micro-channels.[2] This has prompted many studies to investigate velocity slip in the context of microfluidics. The velocity slip can be an intrinsic slip due to chemical coating on a surface (e.g., Ref. 3) or an effective slip due to micro-patterning on a superhydrophobic surface (e.g., Refs. 4–9) or lubricant-impregnated surface (e.g., Refs. 10 and 11). A superhydrophobic surface is a micro-textured surface with trapped gas as the lubricating phase, for which the liquid–gas interface is often modeled as a perfect slip boundary (e.g., Ref. 12).

Experimental evidence has pointed to the possibility of changing the slip condition by ion adsorption for pressure-driven flow of liquids in capillaries. For example, Kiseleva *et al.*[13] discovered an increase in the solution flow rate when they measured the viscosity of cetyltrimethylammonium bromide (CTAB) solutions in micron-sized quartz capillaries. They explained that such an increase in the flow rate might be attributed to slippage of the aqueous CTAB solution over the capillary surface that was hydrophobized as a result of adsorption of the CTA^+ ions from the solution. They also found that similar slippage would occur for flow over methylated quartz surfaces. These findings have led Zhu and Granick[14] to look into if the flow boundary condition could be effectively controlled by the physisorption of surfactant. They conducted experiments to show that dissolving surfactants at dilute concentration in oils could change the hydrodynamic boundary condition of the fluid flow from "stick" to "partial slip." These authors argued that slip effects could arise from the adsorption on solid surfaces of adventitious small amounts of contaminants existing in a fluid.

[a]Author to whom correspondence should be addressed: cong@hku.hk.

As discussed above, the no-slip boundary condition may switch to a partial-slip condition when certain chemical conditions prevailing in the liquid and on the surface are met. While there exist many studies on various aspects (e.g., drag reduction) about wall slippage, the hydrodynamics of flow on the onset of entering a channel bounded by a slippery wall has received little attention in the literature. Davies *et al.*[15] have made an attempt to describe how the near-wall velocity will change in response to the change in the boundary condition in a microchannel with superhydrophobic walls exhibiting ribs and cavities. They postulated that a boundary layer would develop for flow over a no-slip rib, and the growth of the boundary layer would even extend to flow over a partial-slip cavity. This scenario portrayed by Davies *et al.*[15] is, however, not necessarily valid since flow in a microchannel is typically of a low Reynolds number, for which a boundary layer is out of the question. In fact, the problem of flow past a no-slip surface (e.g., a liquid–solid interface at the top of a rib) changing suddenly to flow past a slip surface (e.g., a liquid–vapor interface over a cavity) is not as trivial as it looks. The problem contains elements, such as local stress concentration and sharp pressure gradient, that have not been fully documented in the literature.

In classical hydraulics, the so-called entrance region is well understood. This is a region where the velocity profile evolves from a uniform profile to a parabolic profile (for laminar flow) as the boundary layers develop and extend across the whole channel section. In this classical case, the near-wall fluid particles are retarded as they travel down the channel. The flow is increasingly sheared until it is fully developed. In the present problem, the arrangement is reversed, and in some sense, features show up in the opposite manner. Here, we consider fluid leaving a channel with a no-slip wall for a channel with a partial-slip wall. Therefore, the velocity profile will evolve to a less sheared profile as the flow becomes more uniform under the effect of slip. In this connection, the near-wall fluid particles will accelerate as they traverse the entrance length. In addition, for a low-Reynolds-number flow, the velocity slip will affect fluid particles not only after but also before they enter the slippery channel. The passing of fluid through the cross section where the change in slip occurs (which is a specific axial location termed the slip-change cross section) is at the cost of an additional pressure drop. An objective of this study is to examine how flow is locally disturbed by the sudden change in the slip condition in order to understand the cause of the associated pressure loss.

In previous experiments, data were analyzed many times based on the assumption of a fully developed flow, with the end effect ignored. Many have overlooked the fact that neglecting the end loss can result in appreciable errors when interpreting the data, especially for flow entering a low-friction channel.[16] Another objective of the present study is to obtain results for the local loss, which is expressed in terms of a dimensionless loss parameter that can be readily used to estimate the additional pressure drop incurred by flow crossing a slip-change location. In this paper, the terms "additional loss" and "local loss" are used interchangeably, as either of them refers to the loss of pressure that occurs locally, and in addition to friction loss, owing to the change in the boundary condition. The total loss,

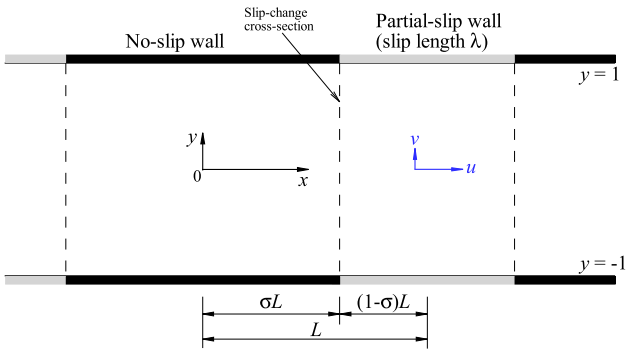

FIG. 1. Flow through a slit channel bounded by walls that are periodically patterned with no-slip alternating with partial-slip transverse stripes. The boundary condition changes from no-slip to partial-slip of slip length λ at $x = \sigma L$, known as the slip-change cross section. All quantities of length dimension are normalized by half the channel height.

which amounts to the applied pressure difference between the two ends of a channel, is the sum of friction and local losses. Specifically, the additional loss under consideration is relative to the pressure drops due to a no-slip channel of length σL and a partial-slip channel of length $(1-\sigma)L$; see Fig. 1. Nevertheless, our dimensionless loss parameter is independent of these two lengths when these lengths are sufficiently large.

We shall further describe the present problems and provide their mathematical formulation and solutions in Sec. II. Two kinds of channels, namely, parallel-plate and circular channels, are considered. Following the Navier slip condition, we assume that the slip velocity is linearly proportional to the near-wall velocity gradient, where the constant of proportionality is known as the slip length. Further assuming Stokes flow and periodic wall patterning, we may solve the problems using the method of eigenfunction expansions, where the unknown coefficients in the series solutions can be determined by imposing the mixed no-slip and partial-slip conditions at discrete points on the boundary. Results are then presented and discussed in Sec. III, where details of the flow field in terms of pressure, wall stress, and vorticity are examined. Velocity profiles at various axial positions are also presented in order to show the existence of an entrance region downstream from the slip-change cross section. The entrance length, which is defined in terms of the attainment of the fully developed momentum correction factor, is found to vary only weakly with the slip length. A dimensionless loss parameter can be used to represent the associated pressure loss. We shall show that this loss parameter depends solely on the slip length if the length of the channel is longer than the entrance length.

II. PROBLEMS AND SOLUTIONS

A. Slit channel

We first consider the pressure-driven flow through a parallel-plate channel, which is made up of two slit channels of the same geometry but different slip conditions joined together. The objective is to find out how the flow will be locally affected by the sudden change in the boundary condition from being no-slip to partial-slip on the walls. We shall refer to the specific axial location where the sudden change in the slip condition

occurs as the slip-change cross section and the point on the wall where the slip change occurs as the slip-change point. Our aim is to determine the pressure loss undergone by the flow on passing through the slip-change cross section.

While the actual channel has two segments and one slip-change cross section, we consider, for the sake of analysis, an extended channel where these segments repeat themselves periodically. Such periodicity will simplify the expression for the solution, as given below. As shown in Fig. 1, we assume in our model that the channel is infinitely long, and its walls are periodically patterned, with no-slip walls alternating with partial-slip walls. Hence, there are infinitely many slip-change cross sections in the channel. Nevertheless, when the period is progressively lengthened, the mutual influence of neighboring units will vanish progressively. The head loss due to the sudden change in the wall slip occurring within a long enough period will be essentially the same as that in the actual non-periodic channel. A similar approach of using a periodic structure to model a non-periodic structure has been used by Laplace and Arquis.[17]

Figure 1 shows one period of the channel, where half the channel height, h, is used as the length scale to normalize all length quantities. The normalized length of a period is $2L$, of which a fraction of $0 \le \sigma \le 1$ is a region of no-slip wall, and a fraction of $1-\sigma$ is a region of a partial-slip wall of slip length λ. The x-axis is along the centerline of the channel, and the y-axis is positioned at the center of the no-slip region. The axial and transverse velocities, denoted by (u, v), are normalized by $K_x h^2/\mu$, while the pressure p is normalized by $K_x h$, in which $-K_x < 0$ is the applied pressure gradient, h is half the channel height, and μ is the dynamic viscosity of the fluid.

By virtue of periodicity and symmetry, it suffices for us to consider the flow in a domain of half period: $0 \le x \le L$, in which the length of the no-slip channel is $L_{\mathrm{NS}} = \sigma L$ and that of the partial-slip channel is $L_{\mathrm{PS}} = (1-\sigma)L$. The model in principle admits any value of $L > 0$ and $0 \le \sigma \le 1$. However, we shall consider only cases where $L_{\mathrm{NS}} = \sigma L \ge 1$ for negligible mutual influence of neighboring units, as remarked above. Typically, it is desired that the no-slip and partial-slip channels are both long enough for a fully developed flow to be established in the middle of each of them, for which $L > 1$ and an intermediate value of σ not too close to 0 or 1 should be considered.

Assuming the incompressible Stokes flow, the governing equations in a dimensionless form are

$$\frac{\partial u}{\partial x} + \frac{\partial v}{\partial y} = 0, \tag{1}$$

$$\frac{\partial^2 u}{\partial x^2} + \frac{\partial^2 u}{\partial y^2} = -1 + \frac{\partial p_i}{\partial x}, \tag{2}$$

$$\frac{\partial^2 v}{\partial x^2} + \frac{\partial^2 v}{\partial y^2} = \frac{\partial p_i}{\partial y}, \tag{3}$$

where p_i is the internally induced pressure.

Using eigenfunction expansion, the velocities and pressure satisfying the equations above and periodicity in the x-direction are expressible as follows:[18]

$$u(x,y) = \frac{1}{2}\left(1-y^2\right) + A_0 + \sum_{n=1}^{\infty} A_n \frac{\cos(\alpha_n x)}{\cosh(\alpha_n)} \left[\cosh(\alpha_n y) - \tanh(\alpha_n)\left(\frac{\cosh(\alpha_n y)}{\alpha_n} + y\,\sinh(\alpha_n y)\right)\right], \tag{4}$$

$$v(x,y) = \sum_{n=1}^{\infty} A_n \frac{\sin(\alpha_n x)}{\cosh(\alpha_n)} \left[\sinh(\alpha_n y) - y\,\tanh(\alpha_n)\cosh(\alpha_n y)\right], \tag{5}$$

$$p(x,y) = -x + p_i(x,y) = -x - 2\sum_{n=1}^{\infty} A_n \frac{\sin(\alpha_n x)}{\cosh(\alpha_n)} \tanh(\alpha_n)\cosh(\alpha_n y), \tag{6}$$

where $\alpha_n = n\pi/L\,(n = 1, 2, \cdots)$ are the eigenvalues and $A_{0,1,2,\cdots}$ are undetermined coefficients. These expressions are derived based on the following considerations and steps. First, the present linear problem is solvable by the finite Fourier transform method,[19] and the solution to the differential equations is termed an eigenfunction expansion. By virtue of the symmetry in geometry, the axial velocity u is an even function of both x and y, while the transverse velocity v is an odd function of both x and y. It then follows from the momentum equations that the pressure p is an odd function of x but an even function of y. The periodicity then enables us to use either sine or cosine eigenfunction of x to represent the axial variations of the velocities and pressure, where the eigenvalues α_n are determined by the condition of vanishing v at $x = 0, L$. Finally, the components that are functions of y can be determined after some algebra upon substituting these eigenfunction expansions into the continuity and momentum equations. On deriving the above expressions, the no-flux condition at the walls, $v = 0$ at $y = \pm 1$, is also used. If the entire channel is non-slippery (i.e., $\lambda = 0$ or $\sigma = 1$), the coefficients $A_{0,1,2,\cdots}$ will be identically zero, leaving behind only the parabolic axial velocity and linear pressure distribution given by the first terms in Eqs. (4) and (6).

The flow is to further satisfy mixed boundary conditions on the wall. At $y = 1$,

$$u = \begin{cases} 0 & 0 \le x < \sigma L \\ -\lambda \frac{\partial u}{\partial y} & \sigma L < x \le L, \end{cases} \tag{7}$$

which on substituting Eq. (4) gives

$$A_0 + \sum_{n=1}^{M} A_n \cos(\alpha_n x)\left[\mathrm{sech}^2(\alpha_n) - \alpha_n^{-1}\tanh(\alpha_n)\right] = \begin{cases} 0 & 0 \le x < \sigma L \\ \lambda + 2\lambda \sum_{n=1}^{M} A_n \cos(\alpha_n x)\tanh^2(\alpha_n) & \sigma L < x \le L, \end{cases} \tag{8}$$

where the coefficients A_n are truncated to M terms. The $M+1$ unknown coefficients $A_{0,1,\cdots,M}$ can be determined using the method of point matching. The domain $0 \le x \le L$ is equally divided into M intervals with $M+1$ grid points located at $x_i = (i-1)L/M$ where $i = 1, \cdots, M+1$. We then enforce the mixed boundary conditions, Eq. (8), to be satisfied at these grid points. In other words, the no-slip condition is to be

satisfied at the first integer $[\sigma(M+1)]$ points, while the partial-slip condition is to be satisfied at the following integer $[(1-\sigma)(M+1)]$ points. The number of points in either the no-slip or the partial-slip part of the domain has to be sufficiently large for an accurate solution to the problem. The point match then forms a system of $M+1$ equations, which can be readily solved using a standard routine for the $M+1$ coefficients. Typically, for σ not too close to 0 or 1, $M \sim 100$ is sufficient to secure good accuracy of the solution.

The rate of flow per unit width of the channel and the section-mean pressure are then found as

$$Q = 2\int_0^1 u\mathrm{d}y = \frac{2}{3} + 2A_0, \tag{9}$$

$$\bar{p}(x) = \int_0^1 p\mathrm{d}y = -x - 2\sum_{n=1}^{M} A_n \alpha_n^{-1} \sin(\alpha_n x)\tanh^2(\alpha_n). \tag{10}$$

The pressure loss from $x=0$ (center of the no-slip region) to $x=L$ (center of the partial-slip region) is equal to $\Delta p = \bar{p}(0) - \bar{p}(L) = L$. Over this length of the channel, the pressure loss can be deemed as the sum of three losses: $\Delta p = \Delta p_{\mathrm{NS}} + \Delta p_{\mathrm{PS}} + \Delta p_{\mathrm{SS}}$, where Δp_{NS} and Δp_{PS} are, respectively, the friction losses over the no-slip and partial-slip parts of the channel, and Δp_{SS} is the additional loss due to the change in the slip condition. To deduce the friction losses, let us recall the following well-known relationships (in terms of the present dimensionless variables) between velocity, flow rate, and pressure gradient for the fully developed Poiseuille flow in a uniform slit channel with wall slip length λ:

$$u(y) = -\frac{\mathrm{d}p}{\mathrm{d}x}\frac{1}{2}\left(1 - y^2 + 2\lambda\right) \quad \Rightarrow \quad Q = -\frac{\mathrm{d}p}{\mathrm{d}x}\frac{2}{3}(1+3\lambda). \tag{11}$$

Since the friction loss is linearly proportional to the length of channel, and Q is independent of the axial position, we may infer from the equation above ($\lambda = 0$ for the no-slip channel) that

$$Q = \frac{2}{3}\frac{\Delta p_{\mathrm{NS}}}{L_{\mathrm{NS}}} = \frac{2}{3}(1+3\lambda)\frac{\Delta p_{\mathrm{PS}}}{L_{\mathrm{PS}}}. \tag{12}$$

From these relations, we may get the two friction losses as follows:

$$\Delta p_{\mathrm{NS}} = \frac{3L_{\mathrm{NS}}Q}{2} = \frac{3\sigma LQ}{2} \tag{13}$$

and

$$\Delta p_{\mathrm{PS}} = \frac{3L_{\mathrm{PS}}Q}{2(1+3\lambda)} = \frac{3(1-\sigma)LQ}{2(1+3\lambda)}, \tag{14}$$

where Q is found using Eq. (9). By the decomposition of the pressure loss into three components, the additional loss can be determined as

$$\Delta p_{\mathrm{SS}} = L - \Delta p_{\mathrm{NS}} - \Delta p_{\mathrm{PS}}. \tag{15}$$

A loss parameter, defined as the additional pressure loss per unit flow rate, is introduced here

$$S \equiv \frac{\Delta p_{\mathrm{SS}}}{Q}. \tag{16}$$

Note that if physical quantities (distinguished by a tilde) are used for the pressure drop and flow rate, the loss parameter is a dimensionless parameter given by

$$S \equiv \frac{h^2 \Delta \tilde{p}_{\mathrm{SS}}}{\mu \tilde{Q}}, \tag{17}$$

where h is half the channel height and μ is the dynamic viscosity of the fluid.

B. Circular channel

We next consider a problem similar to that described above but for a channel of circular cross section. The domain of analysis is shown in Fig. 2, where all the length quantities are normalized by the radius of the channel a. In one period of normalized length $2L$, a fraction of $0 \le \sigma \le 1$ is a region of no-slip wall, and a fraction of $1-\sigma$ is a region of partial-slip wall of slip length λ. By virtue of periodicity and symmetry, it suffices for us to consider the flow in a domain of half period: $0 \le z \le L$, in which the length of the no-slip channel is $L_{\mathrm{NS}} = \sigma L$ and that of the partial-slip channel is $L_{\mathrm{PS}} = (1-\sigma)L$.

Assuming the axisymmetric incompressible Stokes flow, the governing equations in the dimensionless form are as follows:

$$\frac{1}{r}\frac{\partial(ru)}{\partial r} + \frac{\partial w}{\partial z} = 0, \tag{18}$$

$$\frac{\partial}{\partial r}\left[\frac{1}{r}\frac{\partial(ru)}{\partial r}\right] + \frac{\partial^2 u}{\partial z^2} = \frac{\partial p_i}{\partial r}, \tag{19}$$

$$\frac{1}{r}\frac{\partial}{\partial r}\left(r\frac{\partial w}{\partial r}\right) + \frac{\partial^2 w}{\partial z^2} = -1 + \frac{\partial p_i}{\partial z}, \tag{20}$$

where (r, z) are the radial and axial coordinates, (u, w) are the radial and axial components of the velocity, and p_i is the internally induced pressure. Note that the velocities and pressure are normalized by $K_z a^2/\mu$ and Ka, respectively, where K_z is the applied pressure gradient, a is the radius of the channel, and μ is the dynamic viscosity of the fluid.

Using eigenfunction expansion, we may express the solution for the velocities and pressure as follows:[20]

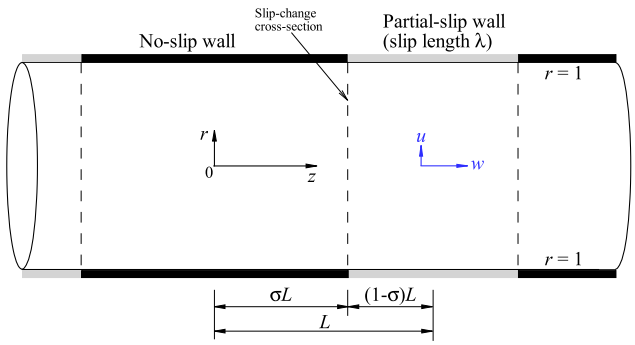

FIG. 2. Flow through a circular channel bounded by a wall that is periodically patterned with no-slip alternating with partial-slip transverse stripes. The boundary condition changes from no-slip to partial-slip of slip length λ at $z = \sigma L$, known as the slip-change cross section. All quantities of length dimension are normalized by the radius of the channel.

$$u(r,z) = \sum_{n=1}^{\infty} A_n \sin(\alpha_n z)\left[\frac{I_1(\alpha_n r)}{I_0(\alpha_n)} - r\frac{I_1(\alpha_n)}{I_0(\alpha_n)}\frac{I_0(\alpha_n r)}{I_0(\alpha_n)}\right], \quad (21)$$

$$w(r,z) = \frac{1}{4}\left(1-r^2\right) + A_0 + \sum_{n=1}^{\infty} A_n \cos(\alpha_n z) \times \left[\left(1 - \frac{2I_1(\alpha_n)}{\alpha_n I_0(\alpha_n)}\right)\frac{I_0(\alpha_n r)}{I_0(\alpha_n)} - r\frac{I_1(\alpha_n)}{I_0(\alpha_n)}\frac{I_1(\alpha_n r)}{I_0(\alpha_n)}\right], \quad (22)$$

$$p(r,z) = -z + p_i(r,z) = -z - 2\sum_{n=1}^{\infty} A_n \sin(\alpha_n z)\frac{I_1(\alpha_n)}{I_0(\alpha_n)}\frac{I_0(\alpha_n r)}{I_0(\alpha_n)}, \quad (23)$$

where $\alpha_n = n\pi/L\,(n = 1, 2, \cdots)$ are the eigenvalues, I_n are modified Bessel functions of the first kind of order n, and $A_{0,1,\cdots}$ are undetermined coefficients. Note that the solution above satisfies the zero-flux condition at the wall $u = 0$ at $r = 1$. These analytical expressions are derived based on steps similar to those outlined above for the preceding problem.

The flow is to further satisfy the mixed no-slip/partial-slip conditions at the wall. At $r = 1$,

$$w = \begin{cases} 0 & 0 \le z < \sigma L \\ -\lambda\frac{\partial w}{\partial r} & \sigma L < z \le L \end{cases} \quad (24)$$

or

$$A_0 + \sum_{n=1}^{M} A_n \cos(\alpha_n z)\left[1 - \frac{2I_1(\alpha_n)}{\alpha_n I_0(\alpha_n)} - \frac{I_1^2(\alpha_n)}{I_0^2(\alpha_n)}\right] = \begin{cases} 0 & 0 \le z < \sigma L \\ \frac{\lambda}{2} + 2\lambda\sum_{n=1}^{M} A_n \cos(\alpha_n z)\frac{I_1^2(\alpha_n)}{I_0^2(\alpha_n)} & \sigma L < z \le L, \end{cases} \quad (25)$$

where the coefficients A_n are truncated to M terms. Again, the $M + 1$ unknown coefficients $A_{0,1,\cdots,M}$ can be determined using the method of point matching, as has been described in Sec. II A. Also, all the coefficients will vanish, $A_{0,1,\cdots} = 0$, when $\lambda = 0$.

After finding the coefficients, we may then evaluate the rate of flow through the channel and the section-mean pressure as

$$Q = 2\pi\int_0^1 wr\mathrm{d}r = \pi\left(\frac{1}{8} + A_0\right), \quad (26)$$

$$\bar{p}(z) = 2\int_0^1 pr\mathrm{d}r = -z - 4\sum_{n=1}^{M} A_n \frac{\sin(\alpha_n z)}{\alpha_n}\frac{I_1^2(\alpha_n)}{I_0^2(\alpha_n)}. \quad (27)$$

The pressure drop from $z = 0$ (center of the no-slip region) to $z = L$ (center of the partial-slip region) is equal to $\Delta p = \bar{p}(0) - \bar{p}(L) = L$. As in the preceding problem, we may consider this pressure loss to be composed of three losses: $\Delta p = \Delta p_{\mathrm{NS}} + \Delta p_{\mathrm{PS}} + \Delta p_{\mathrm{SS}}$, where Δp_{NS} and Δp_{PS} are, respectively, the friction losses over the no-slip and partial-slip parts of the channel, and Δp_{SS} is the additional loss due to the sudden change in the slip condition. To deduce the friction losses, let us recall the following well-known relationships (in terms of the present dimensionless variables) between velocity, flow rate, and pressure gradient for the fully developed Poiseuille flow in a uniform circular channel with wall slip length λ:

$$w(r) = -\frac{\mathrm{d}p}{\mathrm{d}z}\frac{1}{4}\left(1 - r^2 + 2\lambda\right) \quad \Rightarrow \quad Q = -\frac{\mathrm{d}p}{\mathrm{d}z}\frac{\pi}{8}(1 + 4\lambda), \quad (28)$$

from which we may infer that (see the counterpart in Sec. II A)

$$\Delta p_{\mathrm{NS}} = \frac{8\sigma LQ}{\pi} \quad (29)$$

and

$$\Delta p_{\mathrm{PS}} = \frac{8(1-\sigma)LQ}{\pi(1+4\lambda)}, \quad (30)$$

where Q is found from Eq. (26). The additional loss is then determined by subtracting the friction losses from the total pressure loss,

$$\Delta p_{\mathrm{SS}} = L - \Delta p_{\mathrm{NS}} - \Delta p_{\mathrm{PS}}. \quad (31)$$

Again, a loss parameter, or the additional loss per unit flow rate, can be defined as follows:

$$S \equiv \frac{\Delta p_{\mathrm{SS}}}{Q}. \quad (32)$$

Note that if physical quantities (distinguished by a tilde) are used for the pressure drop and flow rate, the loss parameter is a dimensionless parameter given by

$$S \equiv \frac{a^3\Delta\tilde{p}_{\mathrm{SS}}}{\mu\tilde{Q}}, \quad (33)$$

where a is the radius of the circular channel and μ is the dynamic viscosity of the fluid.

III. RESULTS AND DISCUSSION

To gain insight into how pressure varies along the channel, we first show in Figs. 3 and 4 the section-mean pressure $\bar{p}$ as a function of the axial coordinate for the slit and circular channels, respectively, where $\lambda = 0, 0.1, 1, 10$, $L = 2$, and $\sigma = 0.5$. The slip-change cross section, located at the axial position σL, is at the midpoint, $x = 1$ or $z = 1$. In these figures, the actual pressure distributions (solid lines) are shown together with the constructed linear pressure distributions (dashed lines). A constructed pressure distribution is essentially an idealized distribution that is composed of segments of linear pressure distribution as if the flow were everywhere the fully developed Poiseuille flow, with a jump at the location of the slip change. Hence, the segmented linear pressure distribution, which can be obtained by using Eqs. (11) and (28) subject to the boundary conditions $\bar{p}(0) = 0$ and $\bar{p}(L) = -L$, is given by

$$\bar{p}(x) = \begin{cases} -\frac{3Qx}{2} & 0 \le x < \sigma L \\ -L + \frac{3Q(L-x)}{2(1+3\lambda)} & \sigma L < x \le L \end{cases} \quad (34)$$

for the slit channel and

$$\bar{p}(z) = \begin{cases} -\frac{8Qz}{\pi} & 0 \le z < \sigma L \\ -L + \frac{8Q(L-z)}{\pi(1+4\lambda)} & \sigma L < z \le L \end{cases} \quad (35)$$

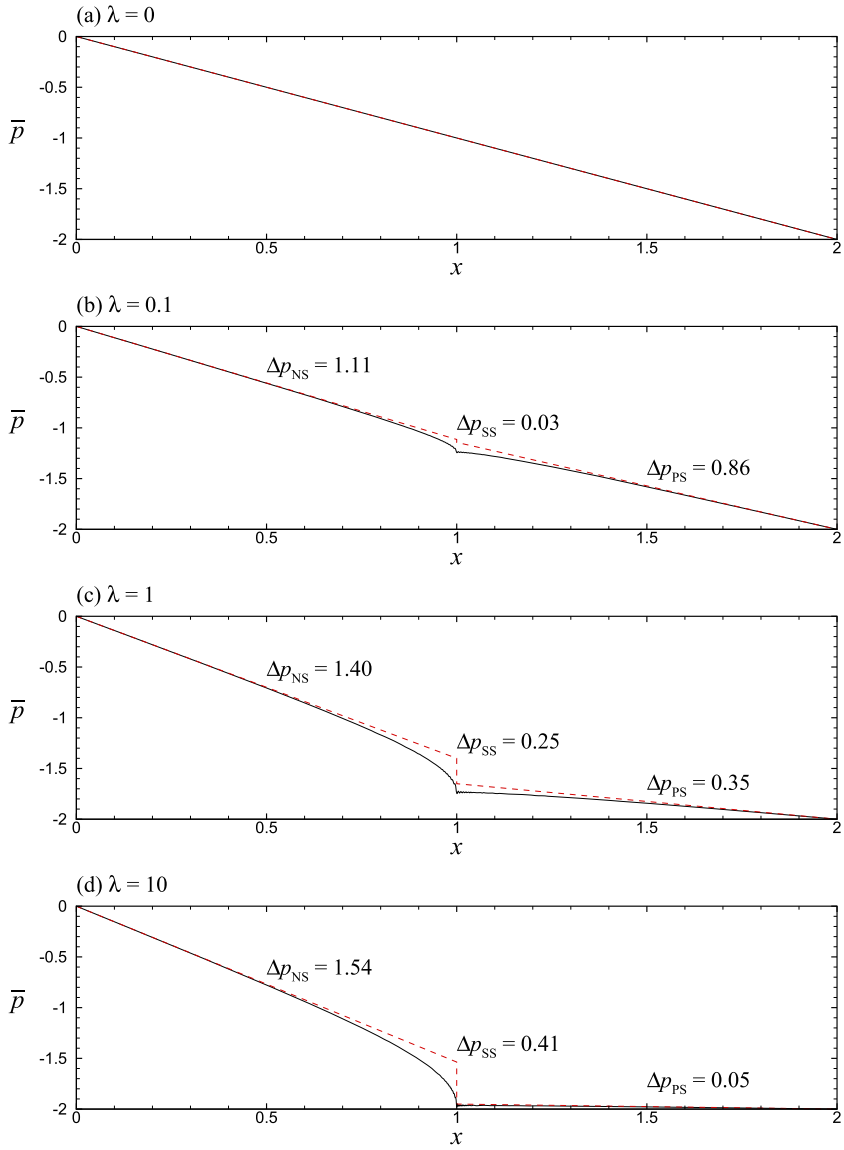

FIG. 3. Axial distributions of the section-mean pressure $\bar{p}(x)$ for flow through a slit channel, where $L = 2$, $\sigma = 0.5$, and (a) $\lambda = 0$, (b) $\lambda = 0.1$, (c) $\lambda = 1$, (d) $\lambda = 10$. The solid lines are the actual pressure distributions. The dashed lines comprise two linear distributions, given by Eq. (34), accounting for the friction loss, and an abrupt drop at $x = 1$, corresponding to the additional loss resulting from the sudden change in the boundary condition at this axial position.

for the circular channel. These two-segment linear distributions would account for the friction losses if fully developed Poiseuille flows could develop from start to end in the no/partial-slip parts of the channel. One can readily check that $\Delta p_{NS} \equiv \bar{p}(0) - \bar{p}(\sigma L)^-$ and $\Delta p_{PS} \equiv \bar{p}(\sigma L)^+ - \bar{p}(L)$ agree with Eqs. (13) and (14) for the slit channel and Eqs. (29) and (30) for the circular channel, respectively. These linear distributions are not continuous at the slip-change cross section for $\lambda > 0$: $\bar{p}(\sigma L)^- \neq \bar{p}(\sigma L)^+$. The jump (in the idealized linear pressure distribution) at this location corresponds to the additional pressure loss Δp_{SS}, as has been given by either Eq. (15) or (31): $\Delta p_{SS} \equiv \bar{p}(\sigma L)^- - \bar{p}(\sigma L)^+ = L - \Delta p_{NS} - \Delta p_{PS}$.

The disturbing effect due to the sudden change in the wall slip is clearly seen in Figs. 3 and 4. The actual pressure distribution will virtually follow the linear distributions (i.e., the flow approximates fully developed Poiseuille flow) at a distance sufficiently far from the slip-change cross section. The pressure will appreciably deviate from the Poiseuille flow pressure only within a finite region before and after the slip-change cross section. This region of pressure deviation, or the extent of local effect, will increase in size, subject to an upper bound, as the slip length increases. The results shown in the figures suggest that, as $\lambda \gg 1$, the local effect arising from the sudden change in the wall slip is largely confined to a distance of ± 0.5 from the point where the slip change takes place. We may say that, in terms of physical dimensions, a distance of $\pm 0.5h$ (for slit channel) or $\pm 0.5a$ (for circular channel) from the slip-change cross section is a range of dominant influence of the change in the slip condition, as far as the section-mean pressure distribution is concerned. The entrance length, which is based on a more precise definition for the development of velocity profile in the slippery channel, is comparable to this distance; see our discussion below.

For $\lambda > 0$, a flow will experience an abrupt change in the axial pressure gradient ($d\bar{p}/dx$ or $d\bar{p}/dz$), from steep to mild, as fluid particles pass through the slip-change cross section; see, e.g., the change in slope of the solid line about $x = 1$ or $z = 1$ in Figs. 3(d) and 4(d). It is remarkable that the pressure gradient becomes very steep as the flow approaches the slip-change cross section. This means that a strong pressure gradient is needed to drive flow approaching a cross section where the slip change occurs.

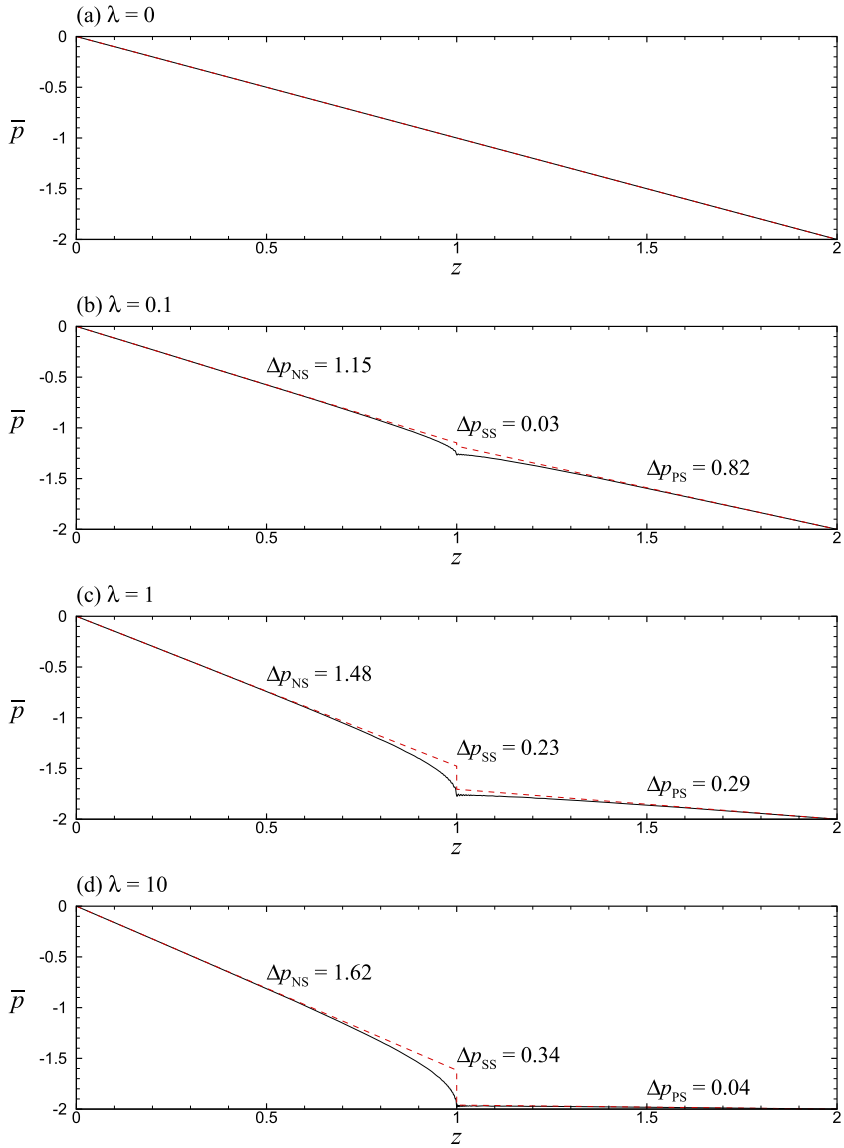

FIG. 4. Axial distributions of the section-mean pressure $\bar{p}(z)$ for flow through a circular channel, where $L = 2$, $\sigma = 0.5$, and (a) $\lambda = 0$, (b) $\lambda = 0.1$, (c) $\lambda = 1$, (d) $\lambda = 10$. The solid lines denote the actual distributions. The dashed lines comprise two linear distributions, given by Eq. (35), accounting for the friction loss, and an abrupt drop at $z = 1$, corresponding to the additional loss resulting from the sudden change in the boundary condition at this axial position.

We also show in Figs. 3 and 4 the values of $\Delta p_{\rm NS}$, $\Delta p_{\rm SS}$, and $\Delta p_{\rm PS}$, corresponding to the friction loss in the no-slip channel, the additional loss at the slip-section cross section, and the friction loss in the partial-slip channel, respectively. These values help us find out how the total loss ($\Delta p = L$) is actually split into the friction and local losses, depending on the slip length λ. It is clearly seen that $\Delta p_{\rm SS} \sim \Delta p_{\rm PS}$ when $\lambda = 1$ and $\Delta p_{\rm SS} \gg \Delta p_{\rm PS}$ when $\lambda = 10$. This means that the local loss arising from the end effect can be comparable to or even much larger than the friction loss for flow through a low-friction channel.

We next show in Fig. 5 the axial distribution of the wall stress τ_w for the same cases as those shown in Figs. 3 and 4. The wall stress is evaluated by $\tau_w = \partial u/\partial y|_{y=1}$ for a slit channel or $\tau_w = \partial w/\partial r|_{r=1}$ for a circular channel. Again, sufficiently far from the slip-change cross section, the wall stress should tend to that of the fully developed Poiseuille flow. Based on the Poiseuille velocity profiles given in Eqs. (11) and (28), the limiting wall stresses can be found as

$$\tau_w = \begin{cases} -\frac{3Q}{2} & \text{(no-slip wall)} \\ -\frac{3Q}{2(1+3\lambda)} & \text{(partial-slip wall)} \end{cases} \tag{36}$$

for the slit channel and

$$\tau_w = \begin{cases} -\frac{4Q}{\pi} & \text{(no-slip wall)} \\ -\frac{4Q}{\pi(1+4\lambda)} & \text{(partial-slip wall)} \end{cases} \tag{37}$$

for the circular channel. Connecting these limiting values is not a smooth stress distribution. Instead, in transition, the wall stress attains a sharp peak slightly upstream of the slip-change cross section. In other words, a flow will experience a sharp increase in the wall stress immediately before it goes past the point where slip change occurs. Inserted in Fig. 5 are the values of the two limiting wall stress magnitudes $|\tau_w|_{\rm NS}$ and $|\tau_w|_{\rm PS}$, and the peak wall stress magnitude $|\tau_w|_{\rm max}$ for the cases shown in the figure. It turns out that, for any $\lambda > 0$, $|\tau_w|_{\rm max} > |\tau_w|_{\rm NS} > |\tau_w|_{\rm PS}$. The peak wall stress can be several times larger in magnitude than the limiting wall stresses. It is remarkable that increasing λ will result in larger $|\tau_w|_{\rm max}$ but smaller $|\tau_w|_{\rm PS}$. As a result, for sufficiently large slip lengths, say $\lambda \geq 1$, $|\tau_w|_{\rm max} \gg |\tau_w|_{\rm PS}$ or a highly concentrated shear stress near the slip-change point. This is another manifestation of the local increase in the resistance to flow associated with the slip change.

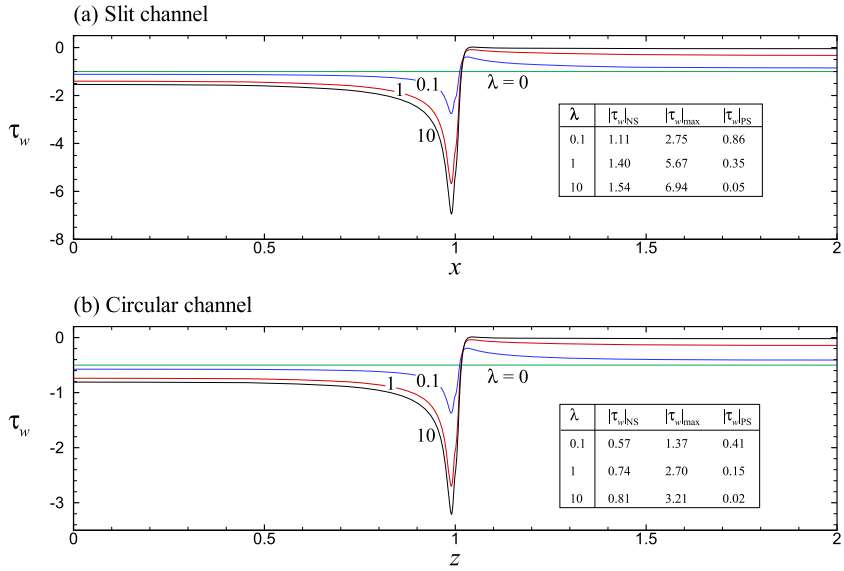

FIG. 5. Axial distributions of the wall shear stress τ_w for flow through a (a) slit channel and (b) circular channel, where $L = 2$, $\sigma = 0.5$, and $\lambda = 0, 0.1, 1, 10$. The boundary condition changes from no-slip to partial-slip at $x = 1$ or $z = 1$. Far upstream and downstream, the wall stress tends to the limiting values given by Eq. (36) for a slit channel and Eq. (37) for a circular channel.

To better understand what causes the local pressure loss, we show in Fig. 6 some further details about the flow through a slit channel for the particular case of $\lambda = 10$. Again, the flow is under the no-slip condition in $x < 1$ and partial-slip condition in $x > 1$. The flow pattern, shown in Fig. 6(a), reveals how a near-wall streamline is displaced toward the wall in the vicinity of $x = 1$. On adjusting itself to satisfy the boundary condition changing from no-slip to partial-slip, the near-wall flow has to undergo acceleration some distance before $x = 1$. This acceleration is not only to increase the axial velocity (a narrower streamtube) but also to induce a transverse flow (a non-parallel streamline) in the neighborhood of $(x, y) = (1, 1)$, which we shall refer to as the slip-change point (i.e., the boundary point of the slip-change cross section). In other words, a fluid particle traveling along this near-wall streamline is not only to gain speed but also to change its direction of motion, when it goes past the slip-change point. To cause such local increase in flow speed, the pressure gradient has to be locally steepened. This explains why the pressure has a sharp dip about the point (1, 1), as is seen in Fig. 6(b). The near-wall flow will be subjected to a very strong pressure gradient on reaching the slip-change point. This strong pressure gradient is to be balanced by a sharp rise in the wall stress, which we have already seen from Fig. 5.

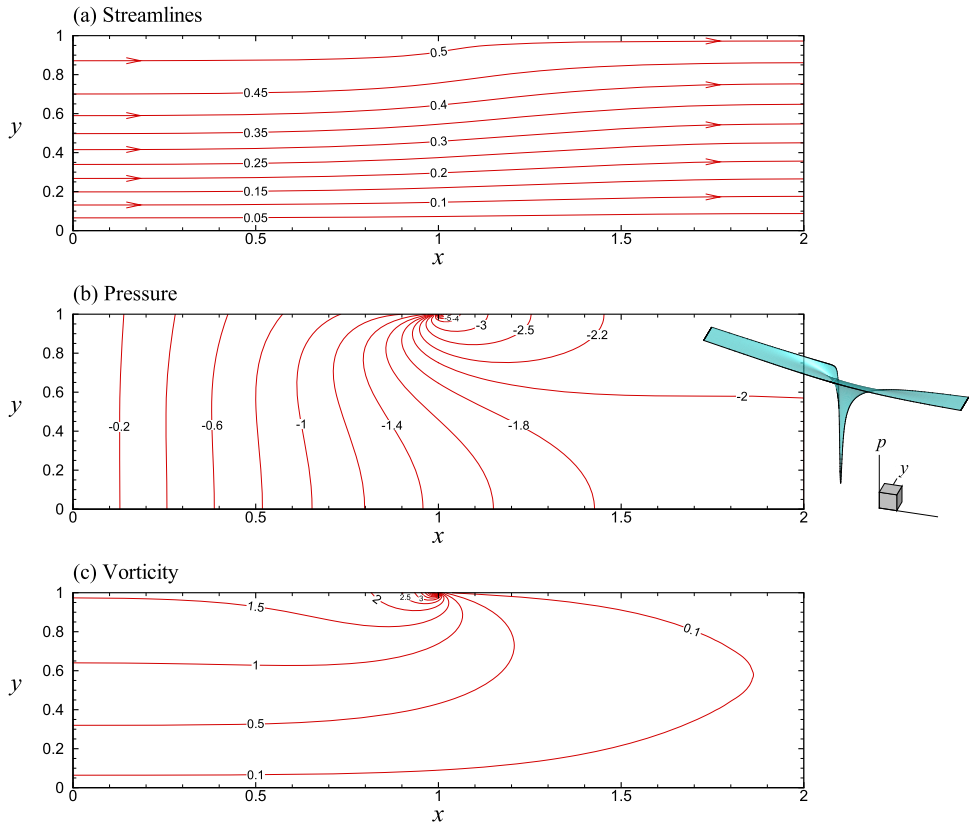

FIG. 6. Two-dimensional plots of (a) streamlines (contour lines of the stream-function $\psi(x, y) = \int_0^y u dy$), (b) pressure field $p(x, y)$, (c) vorticity field $\zeta(x, y) = \partial v/\partial x - \partial u/\partial y$ for flow through a slit channel, where $L = 2$, $\sigma = 0.5$, and $\lambda = 10$. The boundary condition changes from no-slip to partial-slip at $x = 1$. A three-dimensional view of the pressure field is also shown in (b).

It is also of interest to inspect what happens to the pressure and flow fields downstream from the slip-change cross section, say in the region $1 < x < 2$. Figure 6(b) shows that the isobars are mostly non-perpendicular to the x-axis in this region. There exists a pressure gradient in the y-direction that tends to drive flow toward the wall. This transverse flow, albeit small compared with the axial flow, is needed in order to achieve the slip velocity at the wall. A closer inspection of Fig. 6(a) will find that indeed the near-wall streamtube keeps narrowing, while the near-center streamtube keeps widening for $x > 1$. In other words, after crossing the slip-change location, the velocity increases near the wall but decreases near the center as the fluid travels down the channel. This two-dimensional flow structure will persist until the fully developed profile is established; see Fig. 7.

The increase in flow speed, in combination with the induced transverse flow, is to enhance the vorticity as well. As is shown in Fig. 6(c), the vorticity field $\zeta(x, y) = \partial v/\partial x - \partial u/\partial y$ also exhibits a sharp peak near the slip-change point. The flow is strongly rotational in the neighborhood of this point. Figure 6(c) also reveals how vorticity decreases when fluid enters the channel with the partial-slip wall. Here, for $\lambda = 10$, the wall is nearly a no-shear boundary, and hence the flow should be nearly irrotational when fully developed in this part of the channel. From Fig. 6(c), we can see that the vorticity will not diminish to low values until some distance downstream from the slip-change cross section. There are two ways in which we may understand the cause of the local pressure loss. First, a higher pressure gradient than that for the Poiseuille flow is required to drive flow through this region in order that near-wall fluid particles can speed up in response to the change in the boundary condition. Second, maintaining flow in this transition region, which carries more vorticity than the corresponding Poiseuille flow does, is at the cost of an additional pressure drop.

Axial velocity profiles $u(y)$ at axial positions $x = 0.5$, 1, 1.5, 2 for the case of a slit channel are shown in Fig. 7, where the slip-change cross section is located at $x = 1$. As the fluid flows down the channel, the axial velocity will evolve from one limiting profile into another limiting profile, corresponding to the fully developed Poiseuille flow profiles, as given earlier in Eq. (11),

$$u(y) = \begin{cases} \frac{3(1-y^2)Q}{4} & \text{for no-slip wall} \\ \frac{3(1-y^2+2\lambda)Q}{4(1+3\lambda)} & \text{for partial-slip wall,} \end{cases} \tag{38}$$

which are shown by dashed lines in Fig. 7. We can infer from these profiles that the shear rate is always zero at $y = 0$ and maximum at $y = 1$. Hence, much of the viscous diffusion takes place at the wall. Let us assume a sufficiently large slip length, say $\lambda \geq 1$, in the following discussion. As noted above, the near-wall fluid accelerates when approaching the slip-change

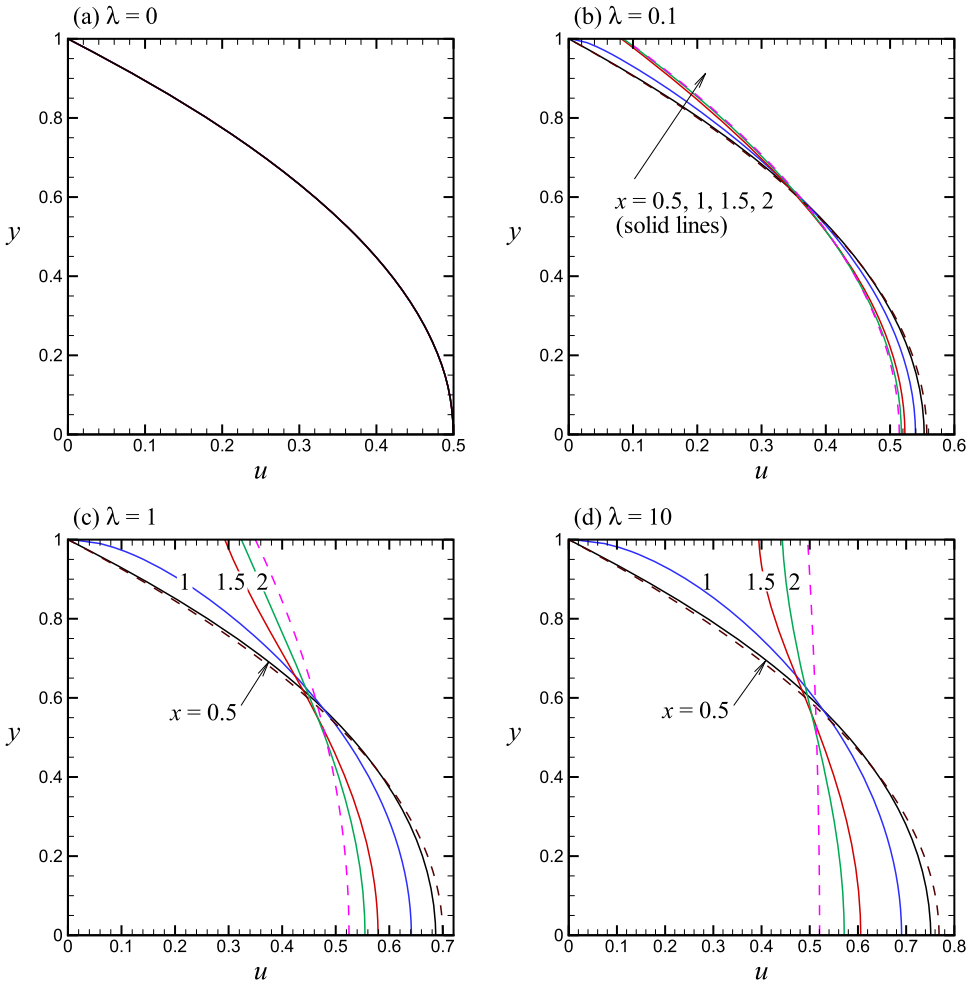

FIG. 7. Profiles of the axial velocity $u(y)$ at $x = 0.5$, 1, 1.5, 2 for flow through a slit channel, where $L = 2$, $\sigma = 0.5$, and (a) $\lambda = 0$, (b) $\lambda = 0.1$, (c) $\lambda = 1$, (d) $\lambda = 10$. The slip-change cross section is at $x = 1$. The dashed lines denote the two limiting fully developed velocity profiles given by Eq. (38).

cross section, but this happens while the flow has still to satisfy the no-slip condition at the wall. The consequence is to steepen the velocity gradient at the wall. Figure 7(d) shows that, for $\lambda = 10$, the velocity gradient $\partial u/\partial y|_{x=1,y=1}$ is indeed very steep. Such a steep velocity gradient amounts to a large shear stress or a large vorticity. This concurs with what we have already seen from earlier figures: fluid particles on getting close to the slip-change point (1, 1) will be subjected to large shear stress and vorticity. The large stress and vorticity, however, cannot be sustained further down beyond this point. Under the slip condition, the slip velocity is in direct proportion to the near-wall velocity gradient. As the slip velocity at the outset is small, the velocity gradient at the wall must therefore drop abruptly to a small magnitude shortly after the fluid passes by the point (1, 1). From $x = 1$ onward, the flow will gradually develop an increasingly uniform velocity profile or a profile of decreasing rotationality. Figures 7(c) and 7(d) reveal that, after entering the partial-slip channel, the fluid has to traverse a certain distance before the final velocity slip at the wall is achieved.

It is noteworthy that in the course of transitioning from the no-slip to the partial-slip profile, a point of inflection may show up in the middle of the velocity profile; see, e.g., the profile at $x = 1.5$ shown in Fig. 7(d). This can be explained as follows. First, the velocity gradient is zero at the center because of symmetry about the centerline. Second, a large slip length leads to a very small wall shear stress or a very small velocity gradient at the wall. As a consequence, the velocity gradient is very small near both $y = 0$ and $y = 1$, and the velocity gradient may attain a maximum (in magnitude) at an intermediate y. This point of the maximum velocity gradient is of course a point of inflection in the velocity profile. This point of inflection also corresponds to a point of maximum shear rate, maximum shear stress, or maximum vorticity over the particular cross section. For fully developed flow, the maximum stress and maximum vorticity are always located at the wall. In contrast, for flow just entering a partial-slip channel, it is possible that the maximum stress and maximum vorticity are located at a point between the wall and the centerline.

We further show in Fig. 8 how the velocity profile develops as a function of $x' = x - \sigma L$, which measures the distance downstream from the slip-change cross section. The cases shown in this figure are for $\lambda = 10$, $L = 10$, and (a) $\sigma = 0.5$ ($L_{PS} = 5$), (b) $\sigma = 0.95$ ($L_{PS} = 0.5$), where $L_{PS} = (1 - \sigma)L$ is the length of the channel with the slippery wall. The axial coordinate is re-defined such that the origin $x' = 0$ is positioned at the slip-change cross section. Here, the slippery channel is long enough in case (a), but too short in case (b), for the flow to attain the fully developed profile in this channel. The leftmost and rightmost profiles in the figure are the profiles given by Eq. (38) for the fully developed flow in the no-slip and partial-slip parts of the channel, respectively. Provided in the figure are also the percentage values of the slip velocity relative to the final slip velocity. From these values, we can estimate how long a distance from the slip-change cross section is needed for the final profile to be practically attained. Note that the farthest point (i.e., the midpoint of the partial-slip channel at $x = L$ or $z = L$; see Figs. 1 and 2) where the flow can develop to approach the limiting Poiseuille flow is $x' = 5$ in case (a) and $x' = 0.5$ in case (b). In case (a), more than 99% of the slip velocity is already established at $x' = 2$, and virtually 100% of the limiting velocity profile is attained before the farthest point $x' = 5$ is reached. In case (b), the slippery channel is too short for the limiting velocity profile to be established. At the farthest point $x' = 0.5$, only some 60% of the limiting slip velocity can be achieved.

In addition to velocity flow, let us also briefly look into the momentum flow. The momentum flux is equal to (momentum correction factor) × density × (section-mean velocity)^2 × area.[1] The momentum correction factor β, which accounts for non-uniformity of velocity over a cross section, is the only variable depending on the axial position in this equation. It can be found as follows:

$$\beta = \begin{cases} \int_0^1 u^2 \mathrm{d}y/\bar{u}^2 & \text{for slit channel} \\ 2\int_0^1 w^2 r \mathrm{d}r/\bar{w}^2 & \text{for circular channel,} \end{cases} \tag{39}$$

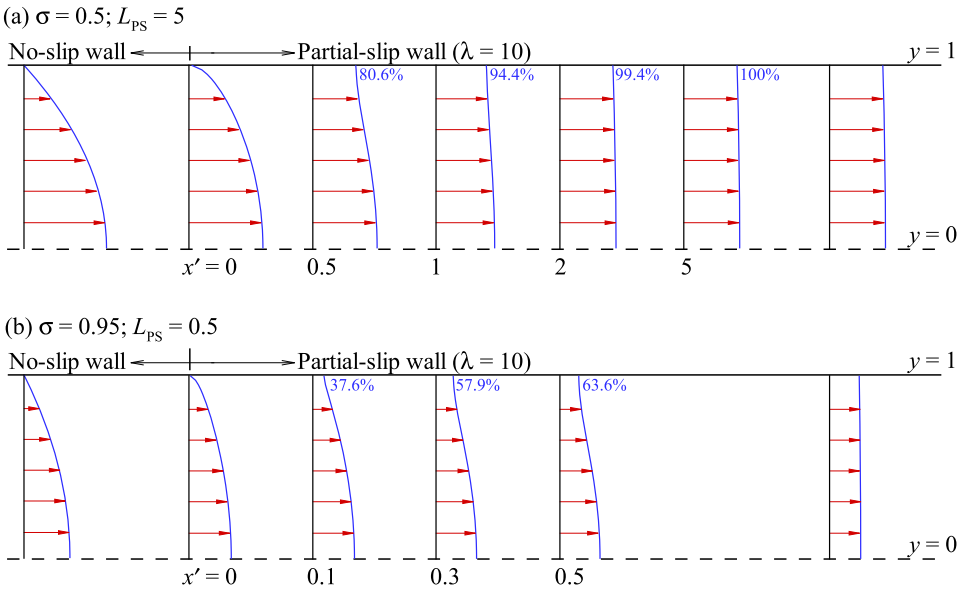

FIG. 8. Profiles of the axial velocity $u(y)$ at various axial positions for flow through a slit channel, where $L = 10$, $\lambda = 10$, and (a) $\sigma = 0.5$ ($L_{ps} = 5$), (b) $\sigma = 0.95$ ($L_{ps} = 0.5$). The axial coordinate $x' = x - \sigma L$ measures the distance downstream from the slip-change cross section. The leftmost and rightmost profiles are the two limiting fully developed velocity profiles given by Eq. (38). The values in percentage are the ratios of the slip velocity to the final slip velocity.

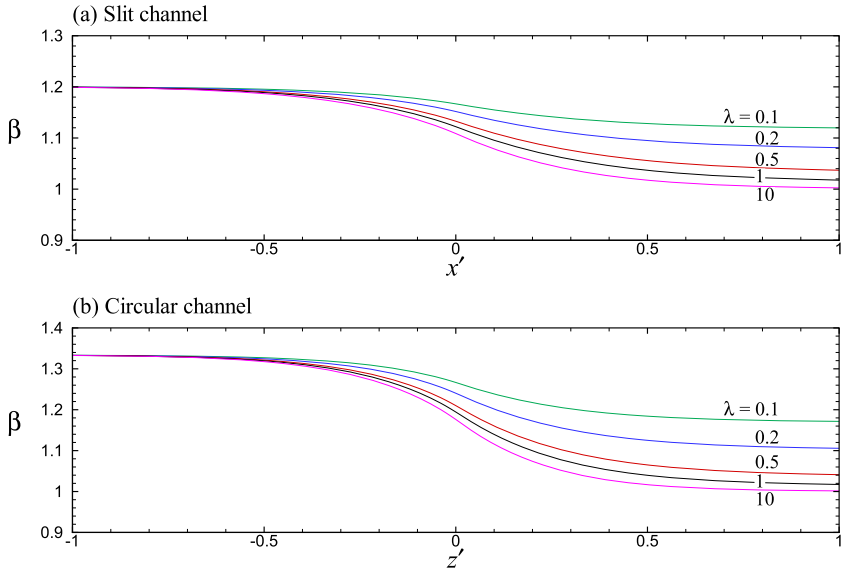

FIG. 9. Axial distributions of the momentum correction factor β for flow through a (a) slit channel and (b) circular channel, where $L = 10$, $\sigma = 0.5$, and $\lambda = 0.1, 0.2, 0.5, 1, 10$. The axial coordinate $x' = x - \sigma L$ or $z' = z - \sigma L$ measures the distance downstream from the slip-change cross section. Far upstream and downstream, the momentum correction factor tends to the limiting values given by Eq. (40) for a slit channel and Eq. (41) for a circular channel.

where $\bar{u}$ and $\bar{w}$ are the section-mean velocities. Substituting the Poiseuille velocity profiles given in Eqs. (11) and (28), we can determine the limiting momentum correction factors to be

$$\beta_{NS} = 6/5, \quad \beta_{PS} = 9\left(\lambda^2 + 2\lambda/3 + 2/15\right)/(1+3\lambda)^2 \qquad (40)$$

for the no-slip and partial-slip parts of the slit channel and

$$\beta_{NS} = 4/3, \quad \beta_{PS} = 16\left(\lambda^2 + \lambda/2 + 1/12\right)/(1+4\lambda)^2 \qquad (41)$$

for the no-slip and partial-slip parts of the circular channel. The momentum correction factor β as a function of the axial coordinate x' or $z' = 0$ and slip length λ is shown in Fig. 9. This factor is identically equal to 1 for a uniform velocity profile, and for any non-uniform profile, it is always greater than 1. For $\lambda > 0$, it is always true that $\beta_{NS} > \beta_{PS} > 1$ as the boundary slip is to result in a more uniform velocity profile. One can readily check that $\beta_{PS} \to 1$ as $\lambda \to \infty$. Unlike the wall stress, the transition of the momentum correction factor (an integral quantity) from β_{NS} to β_{PS} happens in a smooth manner. Even a slip length as small as $\lambda = 0.1$ can appreciably decrease the momentum correction factor by some 10%.

If we regard the flow as fully developed when the momentum correction factor is within 1% of its ultimate value, the "entrance length" L_E can be defined to be the distance from the origin $x' = 0$ or $z' = 0$ to the point where the difference of β and β_{PS} is equal to 1% of β_{PS}. The entrance length L_E defined this way is shown in Fig. 10 as a function of the slip length λ. One can note that over a wide range of slip lengths, from $\lambda = 0.1$ to $\lambda \gg 1$, the entrance length varies only modestly, approximately in the range $0.5 < L_E < 0.8$ for either the slit or circular channel. We may infer from the figure that, for a finite slip length, the fully developed velocity profile with the boundary slip is largely attained within a dimensionless distance of ~0.5 from the entry cross section. In this so-called entrance region, the flow re-organizes itself in order to recover a balance between the axial pressure gradient and lateral viscous momentum diffusion. As seen above, in this transition region, the flow will change to become less sheared or less rotational, as dictated by the boundary slip.

We next show in Fig. 11 the loss parameter, S, which is defined in Eqs. (16) and (32), as a function of the slip length λ,

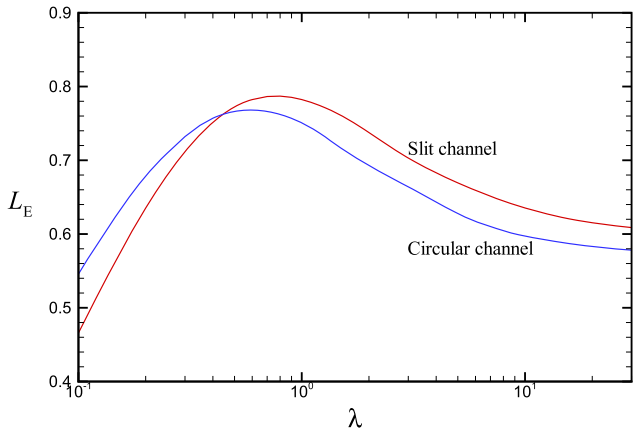

FIG. 10. The entrance length L_E as a function of the slip length λ for flow through a slit or circular channel, where $L = 10$ and $\sigma = 0.5$.

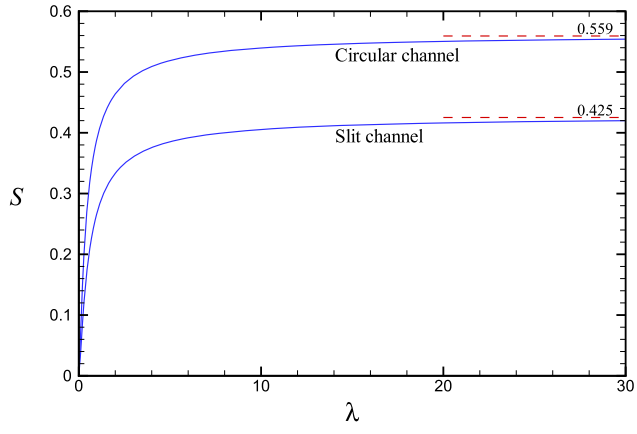

FIG. 11. The loss parameter S as a function of the slip length λ for flow through a slit or circular channel, where $L = 10$ and $\sigma = 0.5$. The dashed lines denote the asymptotic values for very large slip lengths, $\lambda \gg 1$.

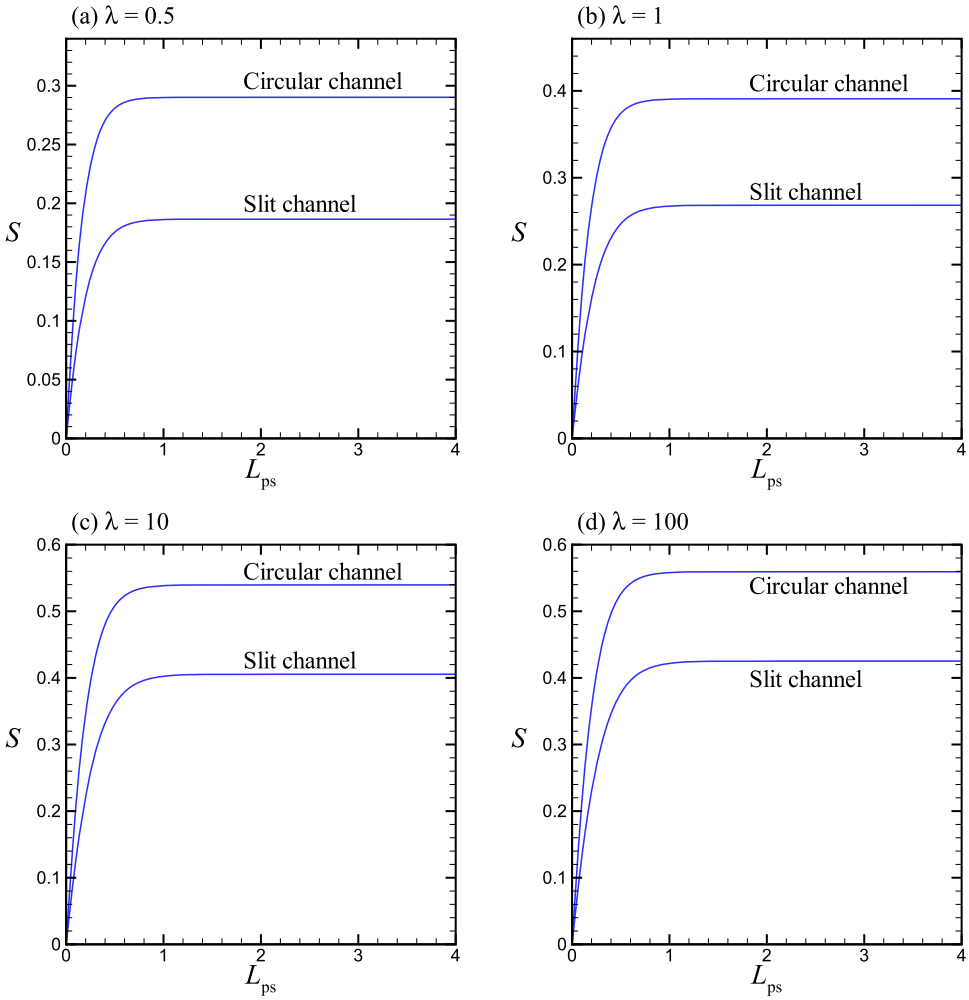

FIG. 12. The loss parameter S as a function of the length of the channel with the slippery wall $L_{ps} = (1 - \sigma)L$ for flow through a slit or circular channel, where $L = 10$ and (a) $\lambda = 0.5$, (b) $\lambda = 1$, (c) $\lambda = 10$, (d) $\lambda = 100$.

where $L = 10$ and $\sigma = 0.5$. The channel is long enough for the fully developed flow to be established in both the no-slip and partial-slip parts of the channel. Hence, the loss parameter is essentially unaffected by other parameters than the slip length λ. The loss parameter is found to increase monotonically with the slip length, which is expected since the additional pressure loss is caused by a sudden change of the slip condition on the wall. The increase of S with λ is quite sharp when λ is small, say $0 < \lambda < 1$. This signifies that even a modest value of the slip length can lead to an appreciable additional loss of pressure. For larger λ, S can only increase mildly with λ. The loss parameter will asymptotically tend to an upper limit for $\lambda \gg 1$. The limiting values, denoted by dashed lines, are provided in Fig. 11. In general, with the same slip length, the loss parameter for flow through a slit channel is smaller than that through a circular channel. This is probably due to the fact that flow in a slit channel is not wall-bounded laterally, while flow in a circular channel is wall-bounded in all directions. Hence, the former is not as susceptible to the wall slip change as the latter.

We finally show in Fig. 12, for various values of λ, the loss parameter S as a function of the length of the channel with the slippery wall $L_{ps} = (1 - \sigma)L$, where $L = 10$. The figure confirms that the loss parameter will not attain its full value until the channel is long enough. In a very short channel, say $L_{ps} < 0.1$, the additional loss can be much reduced. In a sufficiently long channel, say $L_{ps} > 1$, the loss parameter is virtually independent of the length of the channel.

IV. CONCLUDING REMARKS

We have shown that for pressure-driven flow in a slit or circular channel, in addition to the friction loss, there is a pressure drop associated with a sudden change in the boundary condition from no-slip to partial-slip. This additional loss can be represented by a dimensionless loss parameter, defined in Eq. (17) or (33), which is a function of the slip length and does not depend on other physical properties if the channel is longer than the entrance length. One may make use of this loss parameter to evaluate how much additional resistance will be encountered by a flow on entering a channel with a boundary slip. This loss can thus be called an entrance loss. Since the flow under consideration is the Stokes flow, where inertia is neglected, the flow pattern happening at the entrance is exactly the same as that at the exit, with the flow direction being reversed. Hence, the same pressure loss will happen to fluid exiting from the slippery channel. The loss can equally be called an exit loss. In other words, whether it is a change from no-slip to partial-slip or the other way around, the associated pressure loss is the same.

We may extend the present problem to flow entering a slippery channel from a larger reservoir, i.e., flow undergoing

a sudden change in both cross section geometry and slip condition. Sisan and Lichter[16] have studied the end-effects for flow through a low-friction nano-channel. They found that the end losses can have a significant effect on the evaluation of the effective slip length based on the experimental measurement of flow rate and pressure drop. We may look into similar problems of flow in nano-channels and determine how the entrance loss will depend on the slip length, geometrical configurations, and other physical properties. It is also of interest to look into the effect due to inertia at a larger Reynolds number, which may lead to phenomena or features that are dramatically different from those reported in this paper. The problem then becomes nonlinear and has to be solved numerically.

ACKNOWLEDGMENTS

Comments by three anonymous referees are gratefully acknowledged. Financial support by the Research Grants Council of the Hong Kong Special Administrative Region, China, through General Research Fund Project No. 17206615 is also gratefully acknowledged.

[1]B. Massey and J. Ward-Smith, *Mechanics of Fluids*, 8th ed. (Taylor & Francis, New York, 2006).
[2]E. Lauga, M. P. Brenner, and H. A. Stone, *Microfluidics: The No-Slip Boundary Condition* (Springer, New York, 2007), Chap. 19.
[3]C. Cottin-Bizonne, B. Cross, A. Steinberger, and E. Charlaix, "Boundary slip on smooth hydrophobic surfaces: Intrinsic effects and possible artifacts," Phys. Rev. Lett. **94**, 056102 (2005).
[4]J. Ou, B. Perot, and J. P. Rothstein, "Laminar drag reduction in microchannels using ultrahydrophobic surfaces," Phys. Fluids **16**, 4635 (2004).
[5]D. Maynes, K. Jeffs, B. Woolford, and B. W. Webb, "Laminar flow in a microchannel with hydrophobic surface patterned microribs oriented parallel to the flow direction," Phys. Fluids **19**, 093603 (2007).
[6]C. Ybert, C. Barentin, C. Cottin-Bizonne, P. Joseph, and L. Bocquet, "Achieving large slip with superhydrophobic surfaces: Scaling laws for generic geometries," Phys. Fluids **19**, 123601 (2007).
[7]C. J. Teo and B. C. Khoo, "Analysis of Stokes flow in microchannels with superhydrophobic surfaces containing a periodic array of micro-grooves," Microfluid. Nanofluid. **7**, 353 (2009).
[8]C. O. Ng and C. Y. Wang, "Stokes shear flow over a grating: Implications for superhydrophobic slip," Phys. Fluids **21**, 013602 (2009).
[9]A. Busse, N. D. Sandham, G. McHale, and M. I. Newton, "Change in drag, apparent slip and optimum air layer thickness for laminar flow over an idealised superhydrophobic surface," J. Fluid Mech. **727**, 488 (2013).
[10]T.-S. Wong, S. H. Kang, S. K. Y. Tang, E. J. Smythe, B. D. Hatton, A. Grinthal, and A. Aizenberg, "Bioinspired self-repairing slippery surfaces with pressure-stable omniphobicity," Nature **477**, 443 (2011).
[11]B. R. Solomon, K. S. Khalil, and K. K. Varanasi, "Drag reduction using lubricant–impregnated surfaces in viscous laminar flow," Langmuir **30**, 10970 (2014).
[12]A. V. Belyaev and O. I. Vinogradova, "Effective slip in pressure-driven flow past super-hydrophobic stripes," J. Fluid Mech. **652**, 489 (2010).
[13]O. A. Kiseleva, V. D. Sobolev, and N. V. Churaev, "Slippage of the aqueous solutions of cetyltrimethylammonium bromide during flow in thin quartz capillaries," Colloid J. **61**, 263 (1999).
[14]Y. Zhu and S. Granick, "No-slip boundary condition switches to partial slip when fluid contains surfactant," Langmuir **18**, 10058 (2002).
[15]J. Davies, D. Maynes, B. W. Webb, and B. Woolford, "Laminar flow in a microchannel with superhydrophobic walls exhibiting transverse ribs," Phys. Fluids **18**, 087110 (2006).
[16]T. B. Sisan and S. Lichter, "The end of nanochannels," Microfluid. Nanofluid. **11**, 787 (2011).
[17]P. Laplace and É. Arquis, "Boundary layer over a slotted slate," Eur. J. Mech., B: Fluids **17**, 331 (1998).
[18]C. O. Ng and H. C. W. Chu, "Electrokinetic flows through a parallel-plate channel with slipping stripes on walls," Phys. Fluids **23**, 102002 (2011).
[19]W. M. Deen, *Analysis of Transport Phenomena*, 2nd ed. (Oxford, New York, 2012).
[20]H. C. W. Chu and C. O. Ng, "Electroosmotic flow through a circular tube with slip–stick striped wall," J. Fluids Eng. **134**, 111201 (2012).